JOURNAL OF GEOPHYSICAL RESEARCH: EARTH SURFACE, VOL. 118, 2585–2599, doi:10.1002/2013JF002858, 2013

Mean and turbulent velocity fields near rigid and flexible plants and the implications for deposition

Alejandra C. Ortiz,[1,2] Andrew Ashton,[2] and Heidi Nepf[1]

Received 21 May 2013; revised 15 November 2013; accepted 26 November 2013; published 24 December 2013.

[1] The transport of fine sediment and organic matter plays an important role in the nutrient dynamics of shallow aquatic systems, and the fate of these particles is closely linked to vegetation. We describe the mean and turbulent flow near circular patches of synthetic vegetation and examine how the spatial distribution of flow is connected to the spatial distribution of suspended sediment deposition. Patches of rigid, emergent, and flexible, submerged vegetation were considered, with two different stem densities. For the rigid emergent vegetation, flow adjustment was primarily two-dimensional, with flow deflected in the horizontal plane. Horizontal shear layers produced a von Kármán vortex street. Flow through the patch shifted the vortex street downstream, resulting in a region directly downstream of the patch in which both the mean and turbulent velocities were diminished. Net deposition was enhanced within this region. In contrast, for the flexible, submerged vegetation, flow adjustment was three-dimensional, with shear layers formed in the vertical and horizontal planes. Because of strong vertical circulation, turbulent kinetic energy was elevated directly downstream of the patch. Consistent with this, deposition was not enhanced at any point in the wake. This comparison suggests that morphological feedbacks differ between submerged and emergent vegetation. Further, enhanced deposition occurred only in regions where both turbulent and mean velocities were reduced, relative to the open channel. Reduced deposition (indicating enhanced resuspension) occurred in regions of high turbulence kinetic energy, regardless of local mean velocity. These observations highlight the importance of turbulence in controlling deposition.

Citation: Ortiz, A. C., A. Ashton, and H. Nepf (2013), Mean and turbulent velocity fields near rigid and flexible plants and the implications for deposition, *J. Geophys. Res. Earth Surf.*, *118*, 2585–2599, doi:10.1002/2013JF002858.

1. Introduction

[2] The transport of fine sediment and organic flocs plays an important role in the nutrient dynamics of shallow aquatic systems, and the fate of these particles is closely linked to vegetation [*Jones et al.*, 2012; *Larsen et al.*, 2009]. Vegetated regions often contain finer sediment of higher organic and nutrient content than unvegetated regions [*Clarke and Wharton*, 2001; *Larsen et al.*, 2009], and the accumulation of sediment in macrophyte stands can be an important driver in landform evolution [e.g., *Corenblit et al.* 2007]. However, the opposite tendency has also been observed. Specifically, *van Katwijk et al.* [2010] noted that the substrate beneath sparse seagrass meadows was much sandier, with less fine particle and organic matter, than the adjacent bare regions. This can be attributed to the removal of fine and organic material by higher levels of turbulence within sparse meadows [*Luhar et al.*, 2008].

[3] To understand both nutrient dynamics and landform evolution, it is important to understand the biogeomorphic feedbacks that drive macrophyte development, i.e., how changes in vegetation distribution lead to changes in flow distribution that in turn may promote or inhibit additional vegetation growth. Sites of erosion are places of lower nutrient availability that lead to less favorable conditions for plant growth [*Corenblit et al.*, 2007; *van Wesenbeeck et al.*, 2008]. Sites of deposition, where seeds and organic matter accumulate, lead to favorable conditions for plant growth [*Gurnell et al.*, 2001; *Scott et al.*, 1996].

[4] Several previous studies have measured flow and deposition near finite patches of emergent vegetation, i.e., vegetation that occupies the full water depth. The deflection of flow around the patch produces locally enhanced flow at its edges, which promotes erosion, which in turn inhibits the lateral expansion of the vegetation [*Bennett et al.*, 2008; *Bouma et al.*, 2007; *Rominger et al.*, 2010; *Vandenbruwaene et al.*, 2011]. The wake downstream of an emergent patch is a region of elevated suspended sediment deposition [*Chen et al.*, 2012; *Tsujimoto*, 1999] that is also shaded from significant bed load transport [*Follett and Nepf*, 2012], so that the wake is a region of nutrient-rich soil, favorable for new plant growth. Taken together, these two hydrodynamic controls,

[1]Department of Civil and Environmental Engineering, Massachusetts Institute of Technology, Cambridge, Massachusetts, USA.
[2]Department of Geology and Geophysics, Woods Hole Oceanographic Institution, Woods Hole, Massachusetts, USA.

Corresponding author: A. C. Ortiz, Department of Civil and Environmental Engineering, Massachusetts Institute of Technology, Cambridge, MA 02139, USA. (aortiz@mit.edu)

2169-9003/13/10.1002/2013JF002858

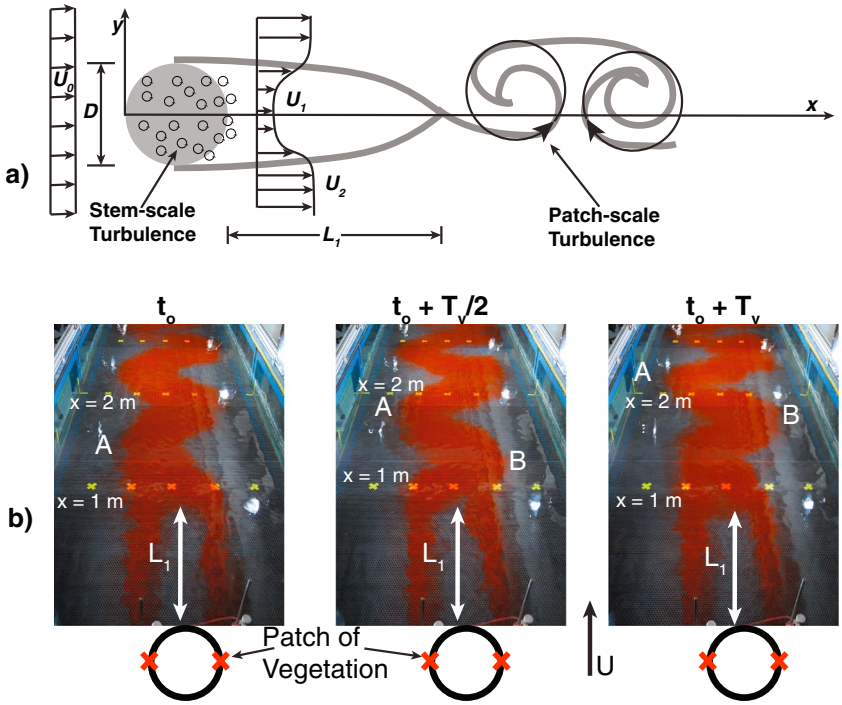

Figure 1. (a) Upstream velocity, U_o, adjusts to patch of emergent vegetation, diameter D, producing a wake profile with velocities (U_1 and U_2) shown with the streamwise, x, and lateral, y, directions. The grey lines represent dye streaks, which appear red in the photos. The steady wake zone is denoted by length L_1. (b) Dye visualization of von Kármán vortex street at starting time, t_o, over one characteristic period, T_v, generated downstream of a dense patch of vegetation, adapted from *Zong and Nepf* [2011]. Two vortices, labeled as A and B, are advecting downstream through time in the three images. Tracer was injected at the red x's. The quiescent region of the wake (L_1) appears as clear water directly downstream of the patch, in between the two dye streaks. The transverse lines of yellow crosses mark 1 m intervals in the streamwise direction.

one that inhibits lateral expansion (a negative feedback) and one that promotes longitudinal expansion (a positive feedback), may explain why patches expand predominantly in the downstream direction. Indeed, *Edwards et al.* [1999] and *Gurnell et al.* [2001, 2005, 2008] observed that fine particle deposition and plant growth in the wake downstream of finite patches of woody debris led to streamlined tree islands. *Schnauder and Moggridge* [2009] suggested that this is an optimal geometry, because it offers a sheltered environment for growth while also minimizing drag during floods. A streamlined geometry has also been observed at smaller scale, for patches of the macrophyte *Callitriche cophocarpa*, which typically have a length that is 2.5 times the width [*Sand-Jensen and Madsen*, 1992]. The positive and negative feedbacks described in this paragraph are drawn from conditions with emergent vegetation. In this study, we consider whether submerged patches provide the same morphological feedbacks. The experiments compare the potential for fine particle and organic matter trapping in the wakes of emergent and submerged vegetation and use detailed measurements of the flow field to explain the differences.

1.1. Wake Downstream of an Emergent Patch

[5] Recent laboratory work has described the flow through and the wake downstream of circular patches of emergent vegetation [*Chen et al.*, 2012; *Follett and Nepf*, 2012; *Zong and Nepf*, 2011]. These studies show that the adjustment of the mean and turbulent flow field depends both on the patch diameter, D, and the density of vegetation within the patch. The density of vegetation is defined by the frontal area per volume, a (cm^{-1}). Given a characteristic stem diameter, d (cm), and the number of stems per bed area, n (cm^{-2}), the frontal area per volume of evenly distributed vegetation is $a = nd$. These two geometric parameters, a and D, together constitute the flow blockage, C_DaD, with C_D the drag coefficient for the individual stems. This parameter determines how the flow adjusts to the patch. Because the patch is emergent, the flow adjustment is essentially two-dimensional in the horizontal plane [*Zong and Nepf*, 2011]. The main features of flow adjustment are shown in Figure 1. A uniform flow characterized by a reference velocity (U_o) approaches the patch from upstream. Deflection of flow around the patch produces a wake in which the velocity is significantly diminished ($U_1 << U_o$), while velocity to the side of the wake is enhanced ($U_2 > U_o$). The magnitude of velocity in the wake, U_1/U_o, can be predicted from the flow blockage, C_DaD [e.g., *Chen et al.*, 2012].

[6] Because some flow passes through the patch, introducing a bleed flow into the wake, the formation of the von Kármán vortex street is delayed, relative to what is observed downstream of a solid obstruction [*Zong and Nepf*, 2010]. The delay has length scale L_1 (Figure 1), and over this distance both the mean velocity (U_1) and the turbulent kinetic energy (TKE) are diminished. The TKE increases rapidly after the vortex street forms, reaching a peak at distance

Table 1. Summary of Experimental Parameters[a]

	Stem Density	aD	H	h	U_o	Wake Velocity	L_1	L_{TKE}
Units	(stems cm^{-2}) ±0.001		(cm) ±0.2	(cm) ±0.2	(cm s^{-1}) ±0.2			
Rigid emergent						U_1 (Figure 1)		
Control	n/a	n/a	13.5	n/a	9.4	n/a	n/a	n/a
Dense	0.34	8.4 ± 0.4	13.5	Emergent		0.5 ± 0.5 cm s^{-1} (0.05 ± 0.05)U_o	2.4D ± 0.2D	3.8D ± 0.5D
Sparse	0.09	2.5 ± 0.1	13.5	Emergent		5.0 ± 0.5 cm s^{-1} (0.53 ± 0.05)U_o	6.6D ± 0.7D	9.5D ± 2D
Flexible submerged						$z/H = 0.3$		
Control	n/a	n/a	21.5	n/a	8.1	n/a	n/a	n/a
Dense	0.34	6 to 34	21.5	10.0		-0.1 ± 0.1 cm s^{-1} (0.01 ± 0.01)U_o	n/a	1.4D ± 0.5D
Sparse	0.09	1.6 to 10	21.5	8.0		1.6 ± 0.1 cm s^{-1} (0.21 ± 0.01)U_o	n/a	1.5D ± 0.5D

[a]Uncertainty in length scales reflects the spatial resolution of measurement. Uncertainty in U_o is instrument error. Uncertainty in wake velocity is the sum of instrument error and standard error over included measurements.

L_{TKE} from the end of the patch. Turbulence production may also occur within the patch, in the wakes of individual stems, if the stem Reynolds number Re_d (= $U_1 d/\nu$, with ν the kinematic viscosity) is above 100 [e.g., *Zong and Nepf*, 2010]. However, because of its small scale, the stem-scale turbulence is rapidly dissipated. Both L_1 and L_{TKE} scale with patch diameter, D, and both L_1/D and L_{TKE}/D decrease as flow blockage ($C_D aD$) increases. Theory developed in *Zong and Nepf* [2011] and *Chen et al*. [2012] can be used to predict L_1 and L_{TKE}.

[7] Dye visualization reveals the von Kármán vortex street downstream of the patch [*Zong and Nepf*, 2011]. Dye is injected at the outermost edges of the patch (Figure 1b). After a distance L_1, the dye streaks come together and a patch-scale von Kármán vortex street forms. Vortices form on alternating sides of the wake, with a characteristic period T_v for one shedding cycle. The period T_v is given by the patch-scale Strouhal number, $St = D/U_o T_v \approx 0.2$ [*Zong and Nepf*, 2011]. In the first frame of Figure 1b (t_o), a vortex has just formed on the left-hand side (labeled A), pulling dye to the left between the 1 m and 2 m markers. In the second frame ($t_o + T_v/2$), vortex A has migrated downstream, and a new vortex (B) forms on the right-hand side. The cycle is completed in the third frame, as a new vortex is again formed on the left-hand side.

[8] Finally, the ratio of patch diameter (D) to channel width (B) can influence the evolution of the wake through its impact on the outer velocity U_2, which increases as D/B increases, because the diverted flow is confined to a narrower width, i.e., (B-D) decreases. As U_2 increases, the length scale L_1 also increases [*Zong and Nepf*, 2011]. This can be observed in Table 1 of *Chen et al*. [2012]. For patches of comparable flow blockage (e.g., $C_D aD = 3.0$ and 3.3) but $D = 22$ and 42 cm, respectively, $L_1/D = 4.5$ and 6.2, respectively.

[9] In contrast to the emergent patch of finite width discussed above, for which flow deflection and wake development occur in the horizontal plane, *Folkard* [2005, 2011] described the flow adjustment over a flexible, submerged patch that spanned the channel width, for which flow deflection occurred only in the vertical plane, forming a vertical shear layer (Figure 2). The vegetation height is h. In the wake of the patch, the shear layer separates, forming a recirculation zone centered at a distance 5 h downstream from the end of the patch. The peak turbulence in the wake occurs at the height of the patch ($z = h$) and a distance 7 h downstream from the patch trailing edge, which also corresponds with the end of the recirculation zone. Following the peak in turbulence, the flow recovers to the boundary layer structure found in open channel flow. In a field study, *Sukhodolova and Sukhodolov* [2012] observed vertical flow adjustment similar to that of *Folkard* [2005], near wide, but not channel-spanning, patches of *Sagittaria sagittifolia*. However, when submerged patches have a width that is much less than the channel width, flow deflection may occur in both the horizontal and vertical planes, e.g., as observed in the field experiments of *Gurnell et al*. [2012].

[10] The pattern of two-dimensional flow adjustment around an emergent patch (Figure 1) has been connected to patterns of erosion and deposition associated with bed load transport [*Follett and Nepf*, 2012] and with net deposition of fine suspended sediment [*Chen et al*., 2012]. In this study, we extend these observations by considering submerged vegetation. In particular, we contrast the flow deflection that occurs for emergent (horizontal deflection only) and submerged (both horizontal and vertical deflection) patches of finite width and explore how these differences impact velocity, TKE, and deposition of suspended sediment. We compare the spatial distribution of deposition to the spatial pattern of mean velocity and TKE.

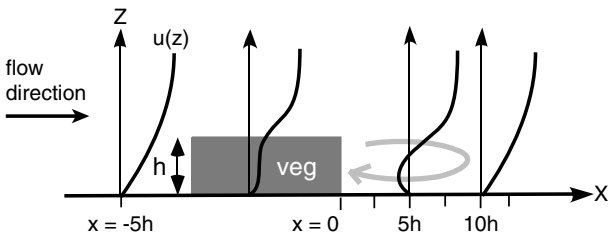

Figure 2. A side view of the flow adjustment over a submerged vegetation patch of height h. The vegetation patch (marked "veg") spans the channel width (into the page), such that all flow adjustment occurs in the vertical plane (x,z). Velocity profiles, $u(z)$, are shown with heavy black curves. The recirculation eddy is shown with light grey arrow. The cartoon is not to scale. Based on *Folkard* [2005, Figures 2a and 3a].

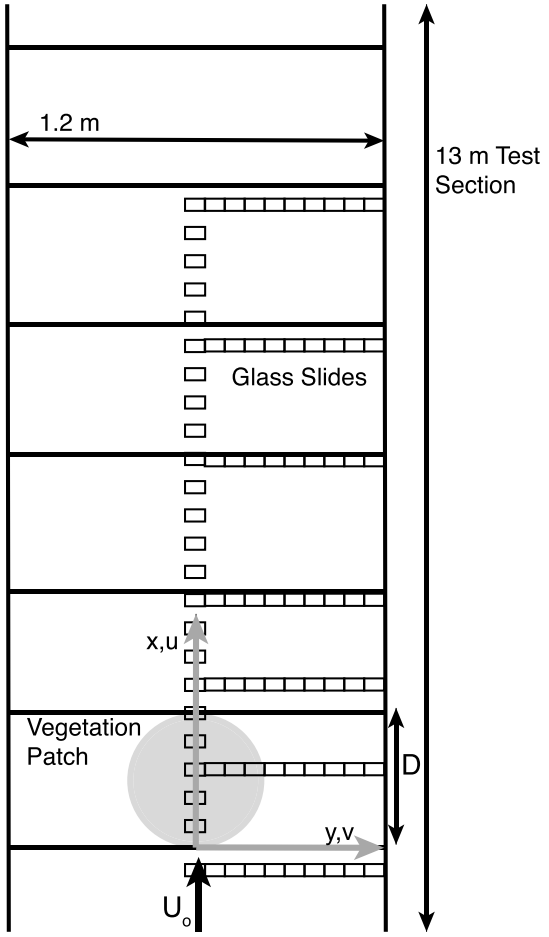

Figure 3. Plan view of the experimental setup in the flume. Model vegetation patch is shown as grey circle. Upstream mean flow (U_o) enters at the bottom of the figure. Microscope slides used for deposition are 7.5 × 2.5 cm and are placed perpendicular to flow. The position of each deposition measurement is recorded in Figure 11.

2. Methods

2.1. Experimental Setup

[11] The experiments were conducted in a 16 m × 1.2 m recirculating flume with a 13 m test section (Figure 3). PVC baseboards, perforated with a staggered array of holes for holding the model vegetation, covered the bed of the test section. There was no sediment layer. A circular patch of model vegetation was constructed at the center of the channel. Wooden, circular dowels with a diameter $d = 6.4$ mm were used for the emergent vegetation. The diameter was chosen to fall in the range of observed values for emergent grasses, $d = 0.1$ to 1 cm [*Leonard and Luther*, 1995; *Lightbody and Nepf*, 2006; *Valiela et al*., 1978]. The flexible vegetation had a 1 cm high stem ($d = 6.4$ mm) with six thin blades of polyethylene film attached as leaves. The flexible model vegetation was dynamically and geometrically similar to the seagrass *Zostera marina* [*Ghisalberti and Nepf*, 2002]. Visual observations in the field suggest that freshwater plants are similar in their response to flow. The individual leaves had a thickness of 0.2 mm, a width of 3 mm, and a length of 13 cm (Figure 4). The diameter of each patch was $D = 42$ cm, chosen to be comparable to field conditions listed in *Sand-Jensen and Pedersen* [2008]. For each type of vegetation, two stem densities were considered, with $n = 0.09$ and 0.34 stems cm^{-2}, which we call sparse and dense, respectively. For the emergent patches and in the stem region of the flexible patches, the solid volume fraction (SVF) is $\varphi = n\pi d^2/4$. For the sparse and dense patches, respectively, $\varphi = 0.03$ and $\varphi = 0.10$. In the blade region of the flexible patch, the range of SVF was estimated by considering the possible range of blades per stem (1 to 6) with full blade width projected to the flow, such that $\varphi = 0.04$ to 0.25 and $\varphi = 0.01$ to 0.07 for the dense and sparse case, respectively. These values of SVF are representative of densities found in real aquatic vegetation [*Nepf*, 2012]. In marsh systems, $\varphi = 0.001$ to 0.01 [*Leonard and Luther*, 1995]. For mangroves φ can be as high as 0.45 [*Furukawa et al*., 1997]. Submerged grasses have ranges of $\varphi = 0.01$ to 0.1 [*Ciraolo et al*., 2006].

[12] Under most conditions, emergent plants have rigid stems and submerged plants have flexible stems, and we mimic this difference in our study. However, a comparison of *Folkard* [2005, 2011], who studied flexible, submerged patches and *Chen et al*. [2013], who studied rigid submerged patches, reveals that the distribution of flow and turbulence in the wake is similar (see discussion in *Chen et al*. [2013]). This makes physical sense, because the vertical shear which drives the wake flow structure develops as a result of flow deflection over the top of the canopy, which is primarily dependent on the canopy density and the ratio of canopy height to water depth [*Chen et al*., 2013]. These studies suggest that the degree of submergence, and not the degree of rigidity, is the dominant control on flow structure of the wake. However, we also note that because flexible plants respond to increasing velocity with increasing pronation, their degree of submergence is dependent on the flow velocity (e.g., see discussion in *Luhar and Nepf* [2011]).

[13] A weir at the end of the flume controlled the water depth, H. For the emergent vegetation, the flow depth was $H = 13.5 \pm 0.2$ cm. A greater depth ($H = 21.5 \pm 0.2$ cm) was needed for the submerged vegetation in order to take velocity measurements above the patch height (h). For the flexible vegetation, the deflected height of the sparse canopy

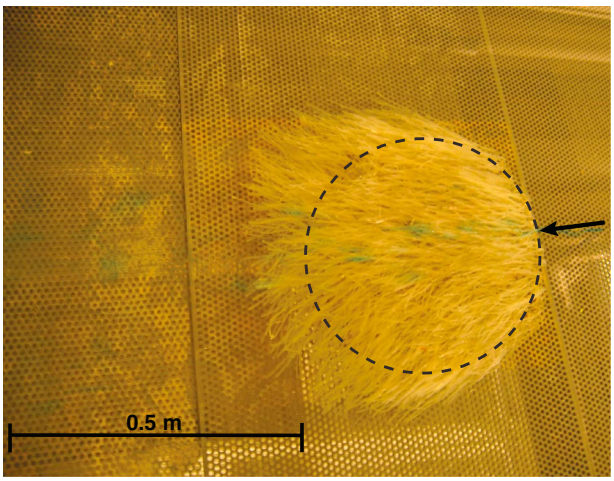

Figure 4. Top view of submerged patch of flexible vegetation in the flume. Flow is from right to left, as indicated by the black arrow. The distribution of cylindrical stems at the bed is outlined with dashed black circle.

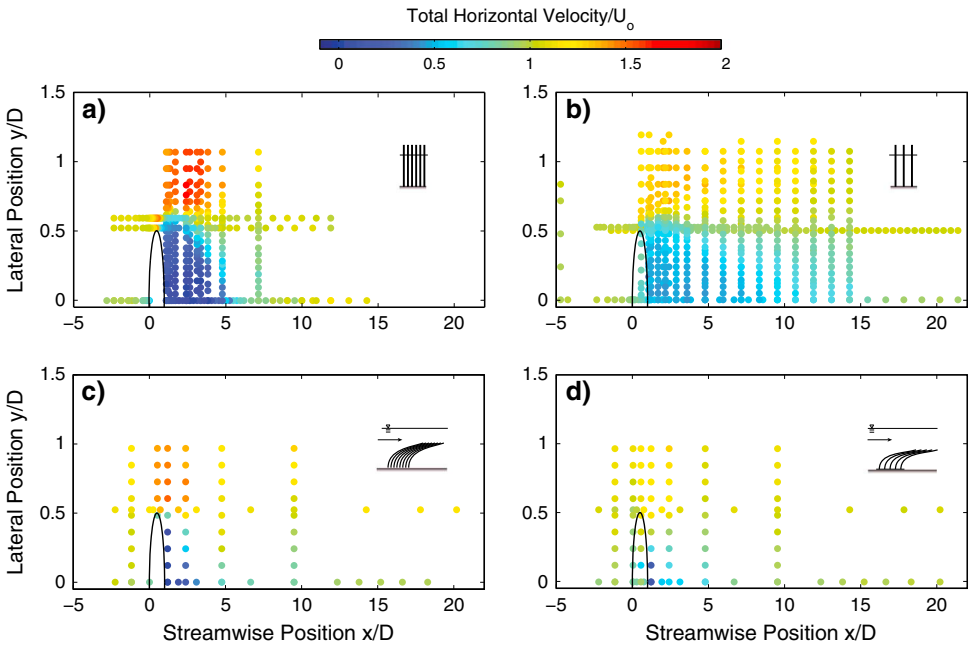

Figure 5. Top view of channel showing the distribution of velocity measurements in the horizontal plane for (a) the dense emergent patch, (b) the sparse emergent patch, (c) the dense submerged patch, and (d) the sparse submerged patch. The color of each dot indicates the magnitude of the total horizontal velocity normalized by U_o, as shown in the color bar. The velocity is measured at the same distance from the bed in all cases: $z = 6.5 \pm 0.5$ cm ($z/H = 0.5$) for the rigid emergent vegetation and $z = 6.7 \pm 0.5$ cm ($z/H = 0.3$) for the flexible, submerged vegetation. The flow is symmetric about the patch centerline ($y = 0$), so that measurements are shown on only one side of the patch. The location of the patch is indicated by a semicircle.

was $h = 8.0 \pm 0.2$ cm. The dense flexible canopy exhibited less deflection due to the greater numbers of blades, such that its deflected height was $h = 10.0 \pm 0.2$ cm.

2.2. Velocity Measurements

[14] The coordinate system is defined with x in the streamwise direction, y cross stream, and z vertical, with $x = 0$ at the leading edge of the patch, $y = 0$ at the center of the patch, and $z = 0$ at the bed (Figure 3). Velocity measurements were taken using a Nortek Vectrino (acoustic Doppler velocimeter, ADV) mounted on a movable platform above the flume and positioned with an accuracy of ±0.5 cm in y and z and ±1 cm in x. Longitudinal transects were taken through the centerline of the patch ($y = 0$) starting 1 m upstream of the patch and extending 7 m downstream beyond the patch ($x = -2.4D$ to $17D$) with variable spacing to increase resolution where velocity variation was more rapid. Lateral transects were taken upstream, at, and downstream of the patch. Figure 5 indicates the position of each velocity measurement.

[15] Velocity was measured at middepth ($z/H = 0.5$) for the rigid emergent patches and at three depths for the flexible, submerged patches, z/H = 0.3, 0.5, and 0.7, which corresponded to midcanopy height, top of the canopy, and above the canopy. For the submerged flexible vegetation, we were unable to obtain measurements within the canopy, because the dense distribution of blades obscured the ADV. The Vectrino collected instantaneous measurements of longitudinal, $u(t)$, lateral, $v(t)$, and vertical, $w(t)$, velocity for 240 s at 25 Hz. The instantaneous velocity was decomposed into time average components (denoted by overbar: $\overline{u}, \overline{v}, \overline{w}$) and fluctuating components (denoted by prime: $u'(t), v'(t), w'(t)$). The turbulent kinetic energy (TKE) per unit mass [*Pope*, 2000] is

$$\mathrm{TKE} = \frac{1}{2}\left(\overline{u'^2} + \overline{v'^2} + \overline{w'^2}\right). \quad (1)$$

[16] A reference velocity, U_o, was defined for the emergent and submerged flow conditions, based on velocity measured for the respective control, i.e., without patch (Table 1). A lateral (y) transect was made at middepth and about 5 m downstream from the start of the test section, which is 1 m upstream from where the patches would be placed. The velocity was uniform over the channel width within the uncertainty (±0.2 cm s^{-1}), and this velocity was chosen as U_o. The reference turbulent kinetic energy (TKE_o) was measured at the same location. Further, vertical profiles taken at this point were uniform above $z = 6$ cm, so that U_o represents the upstream velocity at all three depths used in the submerged flow conditions. Finally, for the emergent patches, the length scale, L_1, was estimated from the centerline transect $\overline{u}(x, y = 0)$ defined by the point at which $\overline{u}$ begins to increase, as in *Chen et al.* [2012]. For all patches, the peak value in TKE downstream of the patch was used to define L_{TKE}.

2.3. Deposition Experiments

[17] We selected model sediment to mimic the transport of organic matter and fine suspended load. The tendency for particles to deposit or resuspend is related to the ratio of the particle settling velocity (w_s) to the shear velocity (u_*, which

represents the velocity scale of turbulent eddies). In aquatic environments, measured settling velocities of organic floc fall around 0.1 to 0.3 cm s^{-1} [*Droppo*, 2004; *Droppo et al*., 1997] and shear velocities range from 1 to 50 cm s^{-1} [*Fuller et al*., 2011; *Hoover et al*., 2010; *Statzner and Mueller*, 1989], yielding ratios of $w_s/u_* = 0.002$ to 0.3. For the lab experiment, we used the bed friction coefficient ($C_f = 0.006$) measured in previous studies over the same baseboards [*White and Nepf*, 2007] and the channel velocity (U_o, Table 1), to estimate $u_* \approx 0.7$ cm s^{-1}. We selected a particle with $w_s = 0.01$ cm s^{-1} (12 μm glass spheres, Potters Industry, Valley Forge, PA), so that $w_s/u_* \approx 0.02$, which is in the middle of the field range. In addition, this ratio is similar to a previous study ($w_s/u_* \approx 0.006$ to 0.2 in *Zong and Nepf* [2010]) in which clear differences in deposition were observed between the open and vegetated regions of a channel. To explore how changes in this ratio impact deposition, we ran additional experiments for $w_s/u_* = 0.008$ to 0.05. We recognize that these ratios imply washload conditions, for which no deposition is expected. However, the ratio represents the channel-average conditions, not the conditions within the patch or patch wake. The study asks whether, or not, finite patches of vegetation can sufficiently reduce local bed stress and turbulent diffusion to allow for local net deposition of fine material and thus verify a critical feedback for vegetation survival, the trapping of nutrient-rich fine and organic matter.

[18] The deposition experiments were conducted separately from the ADV measurements, so that the movement of the ADV would not disturb the deposition slides, but under identical flow conditions. Numbered microscope slides (7.5 cm × 2.5 cm) were placed perpendicular to the flow direction (Figure 3) and at positions every 10 cm along the centerline of the patch, starting 1 m upstream of the patch ($x/D = -2.4$) and ending 6 to 8 m ($x/D = 14.3$–19.0) downstream of the patch. Lateral transects were made at multiple streamwise positions. The position of each deposition measurement is visible in Figure 11.

[19] Once the slides were placed, the pump speed was slowly increased to the target velocity. A total of 650 g of sediment was vigorously mixed with water in small containers before being poured evenly over a 5 min interval into the inlet section of the flume. Visually, the particles mixed almost instantaneously over the water column. The initial sediment concentrations were 105 g/m^3 and 75 g/m^3 for the emergent and submerged vegetation cases, respectively, based on the total mass injected divided by the total flume volume. The experiment was run for 4 h. This duration was chosen by trial and error to be long enough to develop a measurable signal on the slides but short enough to facilitate triplicate runs. At the end, the pump speed was slowly decreased to prevent the formation of long waves that could move the slides. Then, the flume was drained over 20 min. Note that deposition was visually observed to occur progressively over the experimental run and was not isolated to the period of draining. The slides were left to air dry in the flume for 2 to 3 days. Afterward, the slides were placed in a drying oven at 50°C for 2 to 4 h to remove excess moisture and then reweighed. The net deposition on each slide was calculated by the difference in weight before and after the experiment, divided by the area of the slide. Each deposition study was run in triplicate. The standard deviation among triplicates was used as an estimate of uncertainty at each slide position. We also ran control experiments without patches but with the slides at the same positions. The standard deviation of all control points was used as an estimate of uncertainty in the control.

3. Results and Discussion

3.1. Flow Characteristics

[20] The effect of each patch on the horizontal velocity field is depicted with scatterplots of the total horizontal velocity (Figure 5). Because we wish to relate the spatial pattern in flow to differences in net deposition, we chose the measurement closest to the bed and at the same (within uncertainty) distance from the bed for all cases: at $z = 6.5 \pm 0.5$ cm and 6.7 ± 0.5 cm for the rigid emergent and submerged flexible patches, respectively. First, because flow is deflected away from the patch, the velocity directly downstream of each patch (Wake Velocity, Table 1) is diminished relative to the upstream velocity, similar to flow around submerged boulders [*Papanicolaou et al*., 2012], and this effect is more pronounced for the dense patches. Second, the deflection of flow enhances the velocity to the side of all patches ($U > U_o$, Figure 5). This enhancement is greater for the emergent patches, which reach $1.7U_o$ and $1.4U_o$ for dense and sparse conditions, respectively, than for the submerged patches, which only reach $1.5U_o$ and $1.2U_o$ for dense and sparse conditions, respectively. The emergent patches generate a higher edge velocity because flow can only be deflected in the horizontal plane. In contrast, for the submerged patches, flow can be deflected vertically as well. As more flow is deflected over the top of the patch, the acceleration at the edge is decreased. This has important implications for the sediment response. For example, recent studies have noted that elevated velocity at a vegetation edge may produce erosion, a negative feedback for patch growth [*Bouma et al*., 2007; *Rominger et al*., 2010], or changes in sediment texture, as the higher flow preferentially removes fines and leaves coarse-grained sediment [*Sand-Jensen and Madsen*, 1992]. These effects will be more pronounced near emergent vegetation than near submerged vegetation.

[21] For the rigid, emergent patches, the velocity profiles along the centerline of the patch are consistent with the schematic given in Figure 1 and with the two regimes (high and low flow blockage) defined in *Chen et al*. [2012]. The dense emergent patch ($aD = 8.4$) is in the high flow blockage regime, defined as $C_D aD \geq 4$ (assuming $C_D = 1$), for which we expect the velocity directly downstream of the patch to be close to zero, and we expect a flow reversal to occur within the wake. Both features are present in our high flow blockage case (Figure 6a), i.e., directly downstream of the patch $U_1 \approx 0.05U_o$, and an area of flow reversal occurs between $x/D = 3$ and 4. The low velocity, U_1, persists over length scale $L_1 = 100$ cm ($L_1/D = 2.4$, Table 1), ending at the recirculation zone. Within this region, there is both low velocity and low turbulent kinetic energy (Figure 6). Beyond L_1, a von Kármán vortex street forms, enhancing the TKE, which reaches a peak at distance L_{TKE}. The lateral mixing generated by the von Kármán vortices brings high

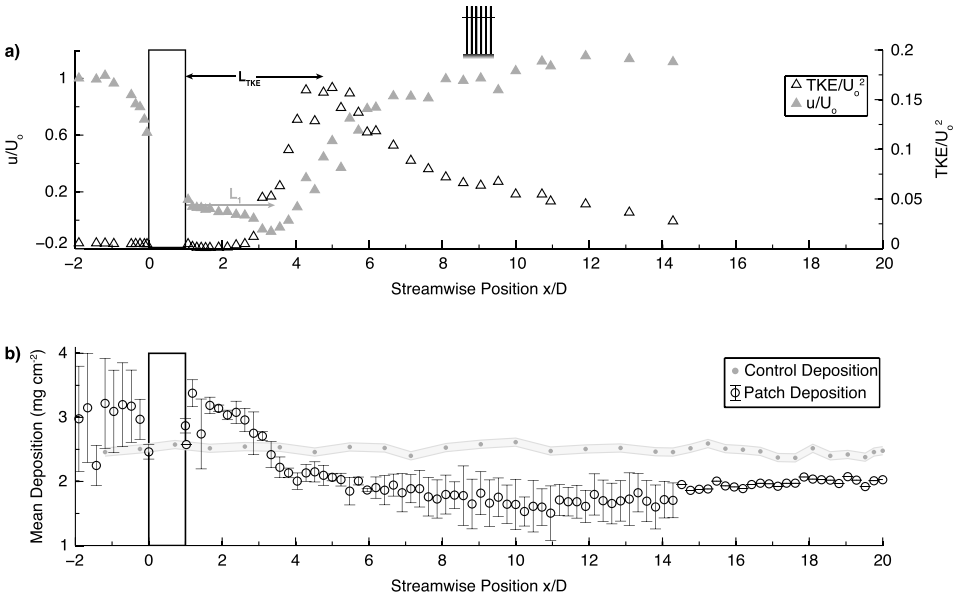

Figure 6. Velocity statistics at middepth ($z/H = 0.5$) and deposition along the patch centerline ($y = 0$) for the dense, rigid, emergent patch of vegetation. The patch is located between $x/D = 0$ and 1, shown by black rectangle. (a) $\bar{u}/U_o$ on the left axis and TKE/U_o^2 on the secondary (right) y axis. Note that TKE/$U_o^2 = 0.013$ at the upstream reference point. (b) Deposition with patch shown by open black circles, with vertical bars indicating the standard deviation among replicates. Deposition in the control (no patch) shown by grey dots, with the gray band indicating the standard deviation among all control points. The distances from the patch trailing edge to vortex formation (L_1) and to the peak turbulent kinetic energy (L_{TKE}) are labeled.

momentum fluid to the centerline, so that the centerline velocity increases, and the velocity eventually returns to the upstream value at $x = 12D$. However, the TKE remains elevated to the end of the measurement region ($x/D = 14$). The longitudinal evolution of the flow in the low flow blockage (sparse) case is similar (Figure 7a), but with the following distinctions. First, compared to a dense patch, the sparse patch allows more flow through the patch, resulting in a larger velocity immediately downstream, $U_1 = 0.5U_o$ (Table 1). A higher exit velocity, or bleed flow, increases the distance to the von Kármán vortex formation [*Chen et al.*, 2012], so that both L_1 and L_{TKE} are greater in the sparse case (Table 1). Finally, there is no area of recirculation.

[22] The flow adjustment around the flexible, submerged patch is fully three-dimensional, with flow diversion and shear layer formation in both the vertical and horizontal

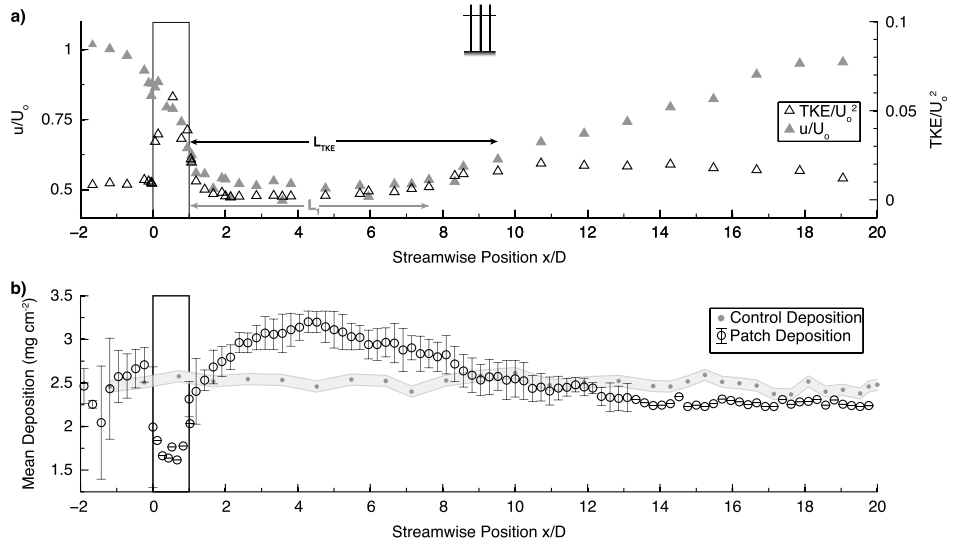

Figure 7. Velocity statistics and deposition measured along the patch centerline for the sparse, rigid, emergent patch of vegetation. See details in caption for Figure 6.

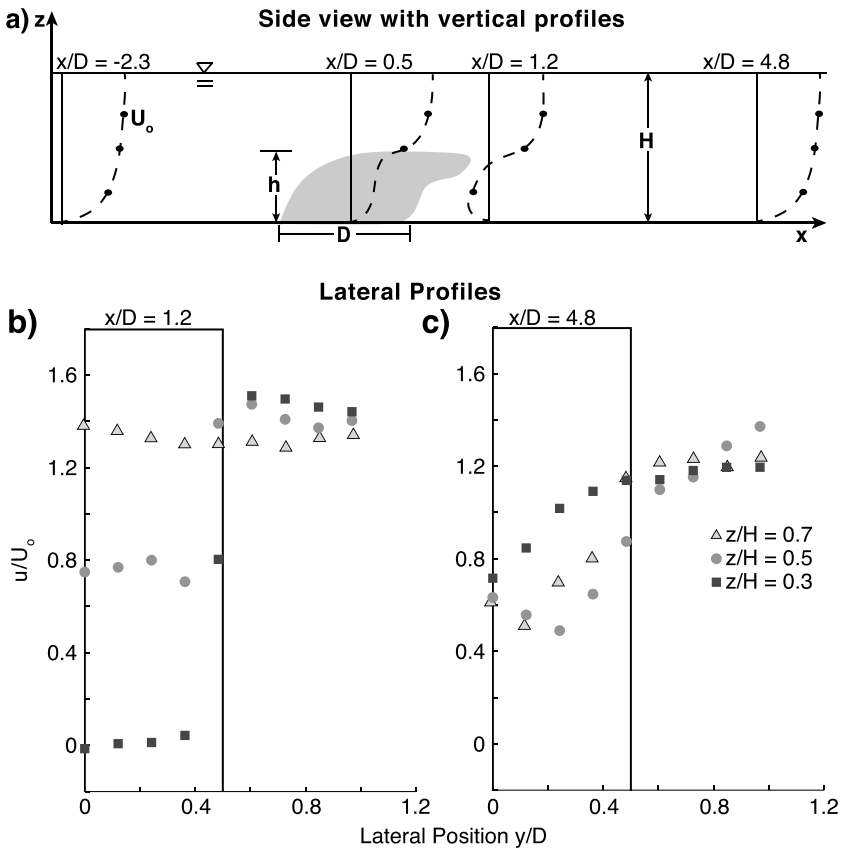

Figure 8. (a) Side view along centerline of dense flexible, submerged patch. Measured streamwise velocity shown with black dots and inferred vertical profiles shown by dashed lines. Note the region of recirculation (negative velocity) at $z/H = 0.3$ and $x/D = 1.2$. (b) and (c) Lateral profiles of streamwise velocity from the centerline (y = 0) to wall at $x/D = 1.2$ (left, b) and $x/D = 4.8$ (right, c) for three vertical positions: $z/H = 0.3$ (square), $z/H = 0.5$ (circle), and $z/H = 0.7$ (triangle). The lateral extent of the patch is denoted by the black rectangle.

planes. For example, consider the dense, flexible, submerged patch (Figure 8). Vertical shear and a recirculation zone are observed in the wake ($x/D = 1.2$ in Figure 8a). At the same position, lateral transects reveal strong lateral shear at $z/H = 0.3$ and 0.5 (squares and dots, respectively, in Figure 8b), with flow diminished ($u/U_o < 1$) directly downstream of the patch ($y/D = 0$ to 0.5) and enhanced ($u/U_o > 1$) at the edge of the patch ($y/D > 0.5$). Above the patch ($z/H = 0.7$, triangles in Figure 8b), the flow is uniformly enhanced ($u/U_o > 1$), with negligible lateral shear. Further downstream (x/D = 4.8) the vertical profile returns to a boundary layer structure (Figure 8a), but the lateral profiles retain evidence of the wake, with reduced velocity persisting at the centerline (y = 0) (Figure 8c). Despite the persistent horizontal shear, there is no evidence for the formation of a von Kármán vortex street. Specifically, dye traces (as in Figure 1) and velocity spectra suggest that a vortex street does not form [*Ortiz*, 2012], possibly because the vertical circulation ($x/D = 1.2$) inhibits the expression of the von Kármán vortex street. For this dense patch, near-bed flow blockage is $C_D aD = 6$ (Table 1), for which a vortex street would not form until $x/D = 2.5$ downstream of an emergent patch [*Chen et al.*, 2012, equation (12)]. If formation scales are similar for a submerged patch, the vertical wake vortex forms before the possible onset of the lateral vortex structures.

[23] Longitudinal transects of mean velocity and TKE taken along the patch centerline further illustrate the flow structure for the flexible, submerged patches (Figures 9 and 10). The flow accelerates over the top of the patch ($z/H = 0.7$, triangle) reaching a maximum just downstream of the patch. The velocity at the height of the patch and within the patch ($z/H = 0.5$, circles, and 0.3, squares) is diminished relative to the upstream flow, such that a region of strong vertical shear exists directly downstream of the patch (also seen in Figure 8). TKE peaks at the height of the patch ($z/H = 0.5$) at $x/D = 2.5$, which corresponds to a distance 6 h downstream of the trailing edge. This is similar to *Folkard*'s [2005] observations downstream of a submerged patch that spanned the channel width. Specifically, Folkard observed a peak in turbulent stress at the height of the patch ($z = h$) and at a distance 7 h downstream from the patch trailing edge. Beyond the point of maximum TKE, the vertical differences in streamwise velocity are erased, i.e., by $x/D \approx 4$ the velocity at all three depths is essentially the same (Figure 9).

[24] If we consider both the similarity in flow structure between our finite width patch and Folkard's channel-spanning

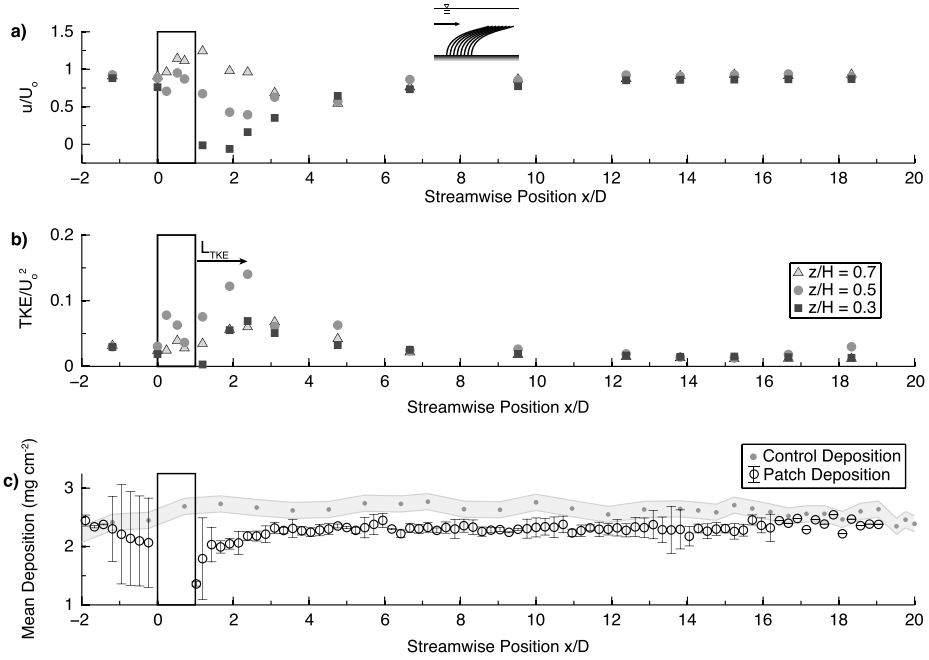

Figure 9. Velocity statistics at three depths ($z/H = 0.3$, 0.5, and 0.7) and deposition along the patch centerline ($y = 0$) for the dense, flexible, submerged patch of vegetation. The patch is located between $x/D = 0$ and 1, shown by black rectangle. (a) u/U_o and (b) TKE/U_o^2 where $\mathrm{TKE}/U_o^2 = 0.026$ at the upstream reference point. (c) Deposition with patch shown by open black circles, with vertical bars indicating the standard deviation among replicates. Deposition in the control (no patch) shown by grey dots, with the gray band indicating the standard deviation among all control points. The distance from the patch trailing edge to the peak turbulence kinetic energy (L_{TKE}) is labeled.

patch, as well as the absence of a von Kármán vortex street, we conclude that for the canopy width to height ratios considered here ($D/h = 4$ and *5*), the flow adjustment more closely resembles that of an infinitely wide ($D/h = \infty$), or channel-spanning patch, i.e., with flow deflection predominantly in the vertical plane. Although not considered in this study, we expect that as D/h decreases, the flow adjustment will become more evenly distributed between the vertical and horizontal. The submergence ratio, H/h, will also play a role in determining the relative importance of vertical and

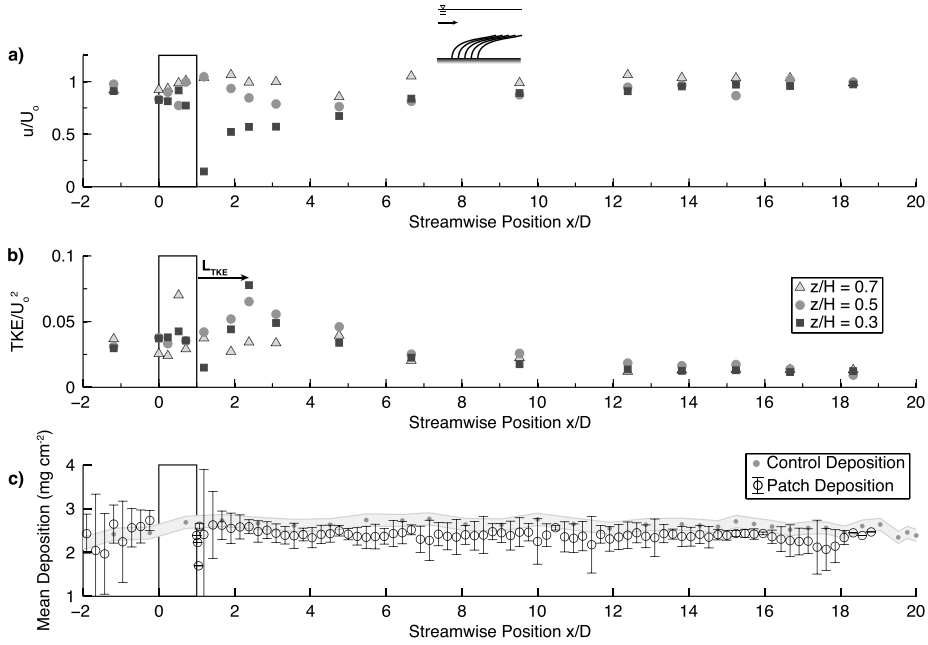

Figure 10. Velocity statistics and deposition measured along the patch centerline for the sparse, flexible, submerged patch of vegetation. See caption for Figure 9. At the upstream reference point $\mathrm{TKE}/U_o^2 = 0.026$.

horizontal deflection. Patches that favor horizontal deflection will produce greater velocity enhancement at the patch edge, which in turn can influence the sediment response, as discussed in Figure 5.

3.2. Sediment Deposition

[25] First, we did not see any indication of supply limitation in the control runs. Specifically, the deposition measured along the centerline for the control condition is reduced by less than 3% along the length of the flume (e.g., see Figure 6). This was expected, because the sediment was remixed each time it passed through the pump, and the time scale for settling ($H/w_s = 3$ to 5×10^3 s) is an order of magnitude longer than the transit time within the measurement section, which spans $L = 10.5$ m [$x = -2D$ to $22D$], so $L/U_o \approx 130$ s. In contrast to the control, deposition measured near an emergent patch had significant spatial variation (e.g., Figures 6 and 7). We note that the spatial variation evolved over the course of the experiment and cannot be attributed to the draining process. While it is difficult to estimate the amount of deposition that occurs during the draining process, any deposition that occurs during draining would be spatially uniform and so cannot explain the spatial pattern of deposition observed for the cases with patches. In addition, the same deposition would occur for control and patch cases, so that the contribution to deposition that occurs during draining is captured in the control.

[26] We compare the spatial patterns of flow and net deposition along the patch centerline (Figures 6, 7, 9, and 10). We first consider the dense, rigid, emergent patch of vegetation (Figure 6b). Deposition upstream of the patch is quite variable between replicates but on average is higher than the control. *Gurnell et al*. [2001] and *Zong and Nepf* [2010] also observed enhanced deposition upstream of a vegetated region and attributed it to the deceleration of flow and the associated decrease in bed shear stress. Downstream of the patch, deposition is enhanced, relative to the control, over a distance comparable to L_1 (marked in figure). Beyond L_1 the deposition is lower than the control, and it remains diminished, relative to the control, to the end of the measurement section ($x = 20D$). The region of diminished net deposition corresponds to the region in which TKE is enhanced by the von Kármán vortex street (Figure 6a), i.e., net deposition varies inversely with TKE. Enhanced deposition occurs where turbulence is low, while reduced deposition (relative to the control) occurs where turbulence is high. We interpret the spatial patterns of net deposition as reflecting differences in resuspension, rather than differences in deposition. During the experimental run, the rate of deposition is the same at all positions in the flume, because the concentration in the water column remains spatially uniform throughout the experiment. Specifically, the deposition is not sufficient within the residence time of the test section to produce significant spatial patterns in water concentration, and each time the water passes through the pumps, the water concentration is completely remixed. However, local changes in flow can create local difference in resuspension. For example, within the emergent patch wake, the velocity and turbulence are reduced, relative to the open channel, which would reduce resuspension, explaining the enhanced net deposited observed in this region.

[27] For the sparse rigid, emergent patch (Figure 7a), L_1 (=6.6D) is longer than for the dense patch, consistent with predictions for $L_1 = f(C_D aD)$ provided in *Chen et al*. [2012]. Importantly, the region of enhanced deposition is also longer, again corresponding with L_1 (Figure 7b). That is, predictable values of $L_1 = f(C_D aD)$ provide a reasonable estimate of the deposition footprint downstream of an emergent patch. Although we considered a single value of D, *Chen et al*. [2012] varied both D and a, showing that $L_1 = f(C_D aD)$ is unique, except through the influence of the sidewalls, expressed through D/B. There are important differences between the dense and sparse emergent cases. First, for the sparse case the upstream deposition is hardly distinguishable from the control, probably because the deceleration of flow and the decrease in bed shear stress is less pronounced for the sparse patch. Second, the decrease in net deposition in the far wake, i.e., beyond L_1, is less pronounced for the sparse patch and in fact very close to the control. This is because the TKE is lower downstream of the sparse patch, so that resuspension is diminished. The peak in TKE is $0.02U_o^2$, which is barely above the open channel control (TKE/$U_o^2 = 0.013$) and much smaller than the peak of $0.16U_o^2$ downstream of the dense patch. Finally, velocity measurements were possible within the sparse patch, and so we can observe that TKE is elevated within the patch. This is due to turbulence generated in the wakes of individual stems, as discussed by *Follett and Nepf* [2012]. Elevated TKE within the sparse, rigid emergent patch explains the significant decrease in deposition both within the sparse patch and immediately downstream of the patch (Figure 7). Although we could not measure inside our dense patch, previous studies have noted elevated TKE and scouring within dense patches as well [*Follett and Nepf*, 2012]. The elevated TKE may promote resuspension of sediment in these areas and, thus, decrease net deposition.

[28] In sharp contrast to the emergent patches, for which regions of enhanced deposition occur downstream of each patch, there are no regions of enhanced deposition in the wakes of the flexible, submerged patches. The deposition is either below the control (Figure 9b, dense patch) or indistinguishable from the control (Figure 10b, sparse patch). This occurs even though the velocity is somewhat lower downstream of the submerged patches, compared to emergent patches of the same near-bed stem density (Table 1). The submerged patches produce recirculation and elevated TKE beginning directly downstream of the patch, with peaks in TKE at $x = 1.4D$ and $1.5D$ for the dense and sparse cases, respectively (Table 1). In contrast, for the emergent patches the peak TKE occurs much further downstream ($L_{TKE} = 3.8D$ and $8D$, Table 1). We suggest that directly downstream from the submerged patches, the net deposition is decreased (relative to the control and relative to the emergent patch) because the TKE is elevated directly downstream of the patch, increasing resuspension. Finally, upstream of the submerged patches the deposition is variable but on average comparable to the control (Figures 9 and 10), which is also a distinction from the enhanced deposition observed upstream of the dense emergent patch. The key point is that unlike the rigid emergent patches, the flexible, submerged patches do not produce enhanced deposition relative to the control experiments.

[29] We now expand our view beyond the centerline transect to consider the broader spatial pattern of deposition (Figure 11). Deposition was classified as equal to the control

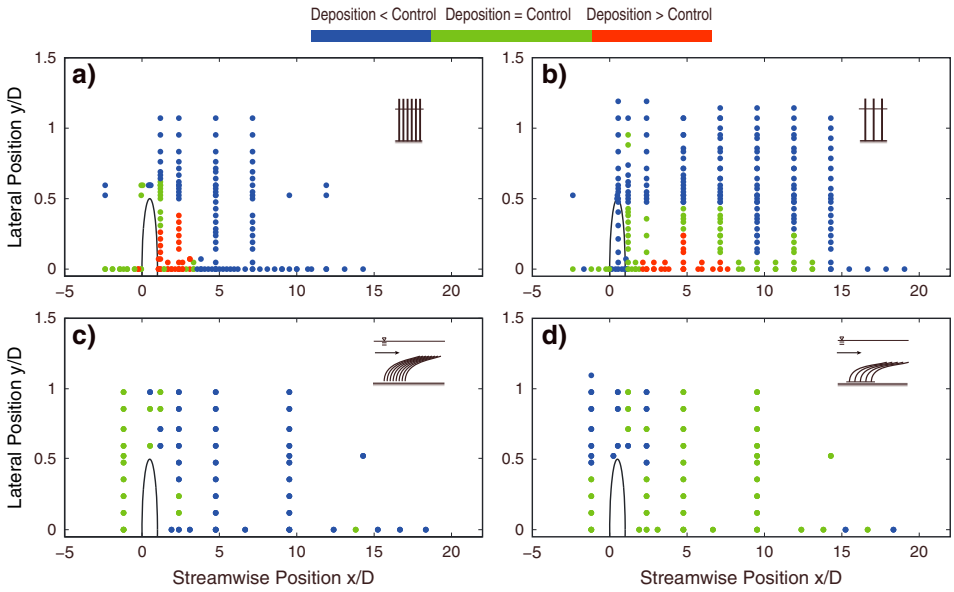

Figure 11. Measured deposition distributed by location in the horizontal plane for (a) the dense emergent patch, (b) the sparse emergent patch, (c) the dense submerged patch, and (d) the sparse submerged patch. Points are colored to indicate magnitude of deposition relative to control, according to color bar. Deposition is considered to be the same as control, if the control plus the control standard deviation lies within the standard deviation of the replicates. The location of the patch is indicated by a semicircle. Flow is left to right, and $y = 0$ is the patch centerline.

if the mean of replicates at a given point agreed with the mean control within the sum of the standard deviation of the replicates and the standard deviation of the control (shown in Figures 6, 7, 9, and 10). Otherwise, the point was labeled as above or below the control. For the emergent patches, deposition above the control occurred within the wake region defined by L_1 (Table 1) and spanning nearly the patch width. It is in this region that both velocity and turbulence are depressed, relative to the open channel control. Deposition is diminished to the side of the patch, corresponding to regions of flow enhancement (see Figure 5). The sparse patch generates a much longer region of enhanced deposition, but it does not span the patch width. Deposition is also diminished within the sparse emergent patch. Deposition measurements were not possible within the other patches. In contrast to the emergent patches, the submerged patches do not generate any locations with deposition elevated above the control.

[30] Both the emergent and submerged patches create regions of diminished velocity, for which we expected enhanced deposition. Yet, enhanced deposition was not always observed. In particular, directly downstream of the submerged patches the velocity is close to zero, yet for the dense submerged patch, this is the point at which the deposition is the lowest (Figure 9). These observations suggest that elevated TKE may play a role. To examine this more closely, we consider the codependence of net deposition on both the time-averaged horizontal velocity and the TKE (Figure 12). Using the same deposition classification as Figure 11, we organize points according to mean velocity (normalized by U_o) and TKE (normalized by U_o^2). The dashed lines indicate velocity and TKE conditions equivalent to the open channel control. The dense, rigid emergent patch produces the largest spatial variability in mean velocity and TKE, reaching maximums of $2U_o$ and 0.2TKE_o. The sparse, flexible, submerged patch produces the smallest flow perturbation, with the smallest ranges of velocity ($0.5U_o$ to $1.2U_o$) and TKE ($0.015U_o^2$ to $0.1U_o^2$). In most cases, enhanced deposition is only observed in the quadrant where both TKE and horizontal velocity are below the open channel values. For the dense patch of rigid emergent vegetation, 89% of the enhanced deposition occurs within this quadrant, and for the sparse patch of rigid emergent vegetation, all of the enhanced deposition (100%) occurs in this quadrant. Note also that there are points within this quadrant without enhanced deposition. This may indicate that we defined the region too conservatively, $u < U_o$ and $\text{TKE} < \text{TKE}_o$, and a less conservative boundary may provide a more precise delineation, e.g., $u \leq 0.5U_o$ and $\text{TKE} \leq \text{TKE}_o$. It may also indicate the importance of particle history, which is not captured in this point analysis, e.g., particles that recently experienced strong turbulence may be mixed high into the water column, and thus less available for deposition. Finally, the occurrences of reduced deposition (indicating enhanced resuspension) are mainly controlled by TKE. Specifically, reduced deposition tends to occur in regions of high TKE, regardless of the mean velocity magnitude (Figure 12).

[31] Currently, most parameterizations of sediment transport depend only on the mean bed stress, which is a function of the mean velocity [*Bos et al.*, 2007; *Christiansen et al.*, 2000; *Rodrigues et al.*, 2006]. However, several studies point to the role of turbulence in initiating sediment motion (resuspension), implying that turbulence can influence net deposition [*Boyer et al.*, 2006; *Celik et al.*, 2010; *Church*, 2006; *Nelson et al.*, 1995; *Nino and Garcia*, 1996; *Williams et al.*, 1989]. Vegetation can alter both the mean and turbulent components of flow [e.g., *Nepf*, 2012], and our observations suggest that changes in both flow statistics influence net deposition.

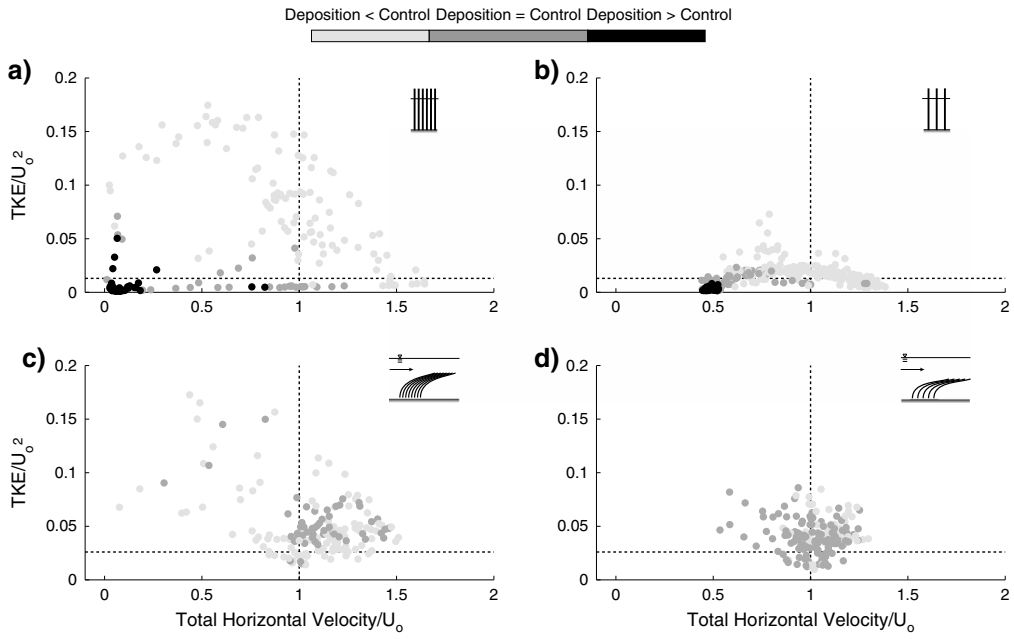

Figure 12. Total horizontal velocity normalized by U_o versus turbulence kinetic energy (TKE) normalized by U_o^2 for (a) the dense emergent patch, (b) the sparse emergent patch, (c) the dense submerged patch, and (d) the sparse submerged patch. Individual points are colored to reflect the net deposition. Deposition is considered to be the same as control if the control plus the control standard deviation lies within the standard deviation of the replicates. The dashed black lines indicate the mean velocity and turbulent kinetic energy of the control experiment.

[32] Previous studies considering emergent vegetation have also observed regions of enhanced deposition in the wake. *Tsujimoto* [1999] observed deposition of fine material downstream of a dense patch of model vegetation. The deposition formed a triangular region that extended a distance 2.5*D* downstream from the back of the patch. *Tanaka and Yagisawa* [2010] observed the preferential deposition of fines in the wakes of real vegetation patches in the field. As noted in section 1, this pattern of deposition in the wake of rigid, emergent vegetation may be connected to the growth pattern of vegetation. During the preliminary stages of colonization, vegetation is often found in circular patches, but over time the patches grow predominantly in the downstream direction [*Sand-Jensen and Madsen*, 1992]. The streamwise growth is promoted by the deposition of fines and organics in the wake of the patch. Our study suggests that this positive feedback will be stronger for sparse emergent patches, which create longer regions of enhanced deposition (Figure 11). Our study also implies that this positive feedback is unlikely to occur for flexible, submerged patches, because we do not observe any preferential deposition in the wakes of the submerged patches (Figure 11). In fact, TKE is elevated so close downstream of the dense flexible, submerged patch that deposition was actually diminished relative to the control. We therefore suggest that patch growth is primarily promoted during low flow conditions, when channel vegetation is emergent, or nearly so. During high flows, which submerge vegetation, the positive feedback for patch growth is shut off. Indeed, the elevated TKE occurring under submerged, high flow conditions may erase deposition occurring in the previous low flow period, suggesting that the timing between high flow events may be critical to patch growth. Low flows, which promote patch growth, must persist for a sufficient time for deposition and germination to occur.

[33] Next, we consider how changes in the velocity ratio w_s/u_* impact the deposition near a dense, rigid, emergent patch. Keep in mind that this ratio, and in particular u_*, represents the open channel, i.e., the conditions away from the patch. Using the same particles (same w_s), we varied the channel velocity, U_o, and thus u_*. For the lowest velocity, ($U_o = 2.6$ and 5.4 cms^{-1}) deposition was not enhanced in the wake (Figure 13a, squares), relative to the open channel adjacent to the patch (Figure 13a, triangle), which is in contrast to the conditions discussed in Figures 6 and 7 ($U_o = 9.6$ cms^{-1}). We interpret this to mean that for these low flow conditions, resuspension in the open channel is sufficiently reduced to be comparable to that occurring in the wake. As U_o increases, resuspension in the open channel increases, leading to a decrease in net deposition adjacent to the patch (Figure 13a). The velocity in the wake, however, remains close to zero for all flow conditions, so that resuspension is unchanged or remains negligible. Because the flume is a closed system, as less material is deposited in the open channel (which represents over 95% of the bed area), more material remains in suspension, available for deposition in the wake. As a result, the deposition in the wake increases with increasing U_o (Figure 13a, squares).

[34] The divergence in net deposition between the patch wake and the adjacent open channel can be captured in a single parameter: the ratio of spatial standard deviation (SD) to the mean (Dep_{mean}) of the measured deposition throughout the flume. The ratio SD/Dep_{mean} is a measure of preferential capture of particles in the patch wake, which increases with increasing channel velocity (Figure 13b). A

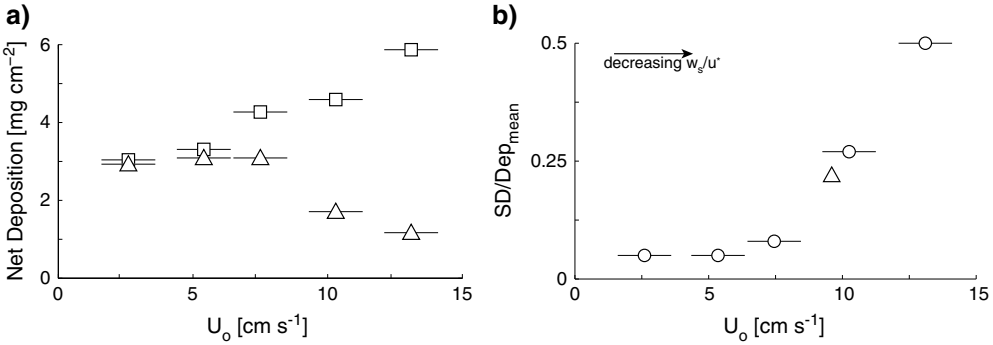

Figure 13. Net deposition near a dense, rigid, emergent patch of model vegetation as a function of channel velocity. (a) Deposition measured adjacent to patch (triangle) and maximum deposition in the wake (square) for $aD = 7$. The uncertainty is comparable to the symbol size. (b) The spatial standard deviation of measured deposition (SD), normalized by the mean deposition (DEP_{mean}) over entire test section. Triangle for $aD = 8.4$ from Figure 6. Additional flow conditions with $aD = 7$ shown by circles. For the additional cases, the estimate of U_o is based on available flow measurements, which did not correspond to the same measurement position for U_o. Uncertainty shown by horizontal bar.

change in behavior occurs around $U_o = 6\ \mathrm{cm\ s^{-1}}$, which corresponds $w_s/u_* \approx 0.01$, and above this value the SD increases rapidly with increasing U_o and continues to increase above our original design conditions (Figure 6, triangle). Although we did not vary w_s, we can use the trends in w_s/u_* to infer deposition behavior. The trend of increasing SD/Dep_{mean} is associated with decreasing w_s/u_* (noted by arrow in Figure 13b). This suggests that within a single system (single value of u_*), preferential deposition in the wake will be stronger (higher SD/Dep_{mean}) for smaller particles (smaller w_s/u_*). This suggestion is supported by observations made by *Tanaka and Yagisawa* [2010], who investigated deposition in the wakes of *Salix subfragilis* patches. They found that the material in the wake was of significantly finer grain material (0.1 to 1 mm) than upstream of the patch (10 to 100 mm), indicating that the preferential capture in the wake was stronger for finer particles. There are two reasons for this. First, as velocity increases, the ability for fines to settle in the open channel (away from the patch) declines more rapidly than in the wake, because the velocity in the wake remains significantly depressed relative to the open channel. Second, because of the depressed velocity in the patch and the wake, the coarse fraction of sediment (bed load) cannot enter the wake. This was shown explicitly in *Follett and Nepf* [2012], who examined a mobile bed with bed load transport interacting with an emergent patch of rigid vegetation. They observed that the coarse fraction of sediment (transported as bed load) did not move into the wake of the patch.

[35] As a final note, we reiterate the fact that our experiments do not include a mobile bed and, thus, cannot represent the influence of bed load transport or changes in bed morphology. As such, the experiments only reveal the initial tendencies for deposition near finite patches of vegetation. However, *Follett and Nepf* [2012] ran experiments on a mobile bed with both bed load and suspended load transport, and they observed deposition of fine material in the wake of a finite patch of emergent vegetation. As noted in the previous paragraph, their study also showed that bed load transport does not occur within the patch wake, which, together with the deposition of fine material, provides good conditions for seed germination and growth. *Follett and Nepf* [2012] observed significant scour at the leading and lateral edges of the patch, processes that are excluded from our study. When present, these changes in bed morphology could inhibit the lateral expansion of the patch and potentially increase the deflection of flow away from the patch, leading to even more quiescent conditions in the wake, and thus more favorable conditions for patch expansion in the streamwise direction.

4. Conclusions

[36] Laboratory experiments examined the alteration of flow and the tendency for suspended sediment deposition of fine particles near finite patches of model vegetation, comparing rigid emergent and flexible, submerged vegetation types. Within the wake of a rigid, emergent patch, there is a distinct region of diminished mean velocity and TKE in which deposition is enhanced. This region extends a distance L_1 downstream of the patch, which can be predicted from the patch flow blockage. The enhanced deposition of fines, in addition to the diminished mean and turbulent flow, could promote germination, seed growth, and, ultimately, patch extension in the streamwise direction. This positive feedback may be stronger for sparse patches, which create longer regions of diminished flow and enhanced deposition, i.e., larger values of L_1. Further, emergent patches deflect flow in the horizontal plane, leading to elevated velocity at the patch edge, which diminished net deposition and may inhibit the lateral expansion of the patch (i.e., a negative feedback to patch growth). In contrast near flexible, submerged vegetation, these feedbacks were greatly reduced or completely absent for two reasons. First, submerged patches do not have a wake region in which both mean velocity and TKE are diminished, and subsequently, deposition is not enhanced downstream of the patch. This suggests that submerged patches do not provide a positive feedback for streamwise patch growth. Second, for submerged patches, flow deflection over the top of the patch diminishes deflection to the side, so that for the same flow conditions, submerged vegetation produces weaker flow enhancement at the patch edge, compared to an emergent patch of comparable stem density. Thus, the tendency to inhibit lateral patch growth and to provoke sediment sorting along the patch edge are likely to be weaker for submerged patches.

Notation List

a	cm^{-1}	frontal area per volume
C_D	~	drag coefficient
C_f	~	bed friction coefficient
d	mm	dowel diameter
D	cm	diameter of patch
h	cm	height of canopy
H	cm	height of water
L_1	m	steady wake length
L_{TKE}	m	length to maximum turbulence
n	cm^{-2}	dowels per bed area
Re_d	~	stem Reynolds number
St	~	Strouhal number
t	s	time
T_v	s	characteristic period of von Kármán vortices
TKE	$m^2 s^{-2}$	turbulence kinetic energy
TKE_o	$m^2 s^{-2}$	upstream reference TKE
U	$cm s^{-1}$	total horizontal velocity
U_o	$cm s^{-1}$	upstream reference velocity
U_1	$cm s^{-1}$	wake velocity
U_2	$cm s^{-1}$	velocity adjacent to wake
u,v,w	$cm s^{-1}$	streamwise, lateral, and normal velocity components
w_s	$cm s^{-1}$	fall velocity
x,y,z	m	streamwise, lateral, and normal directions
φ	~	solid volume fraction (SVF)
v	$cm^2 s^{-1}$	kinematic viscosity

[37] **Acknowledgments.** This material is based upon work supported by the National Science Foundation under grants EAR 0738352 and OCE 0751358. Any opinions, findings, and conclusions or recommendations expressed in this material are those of the authors and do not necessarily reflect the views of the National Science Foundation. We thank Marisa Fryer for her work investigating the effect of varying velocity on the variance of deposition patterns.

References

Bennett, S., W. Wu, C. Alonso, and S. Wang (2008), Modeling fluvial response to in-stream woody vegetation: Implications for stream corridor restoration, *Earth Surf. Processes Landforms*, *33*(6), 890–909, doi:10.1002/esp.1581.

Bos, A. R., T. J. Bouma, G. L. J. Kort, and M. M. van Katwijk (2007), Ecosystem engineering by annual intertidal seagrass beds: Sediment accretion and modification, *Estuar. Coast. Shelf Sci.*, *74*(1-2), 344–348, doi:10.1016/j.ecss.2007.04.006.

Bouma, T. J., L. A. van Duren, S. Temmerman, T. Claverie, A. Blanco-Garcia, T. Ysebaert, and P. M. J. Herman (2007), Spatial flow and sedimentation patterns within patches of epibenthic structures: Combining field, flume and modeling experiments, *Cont. Shelf Res.*, *27*(8), 1020–1045, doi:10.1016/j.csr.2005.12.019.

Boyer, C., A. G. Roy, and J. L. Best (2006), Dynamics of a river channel confluence with discordant beds: Flow turbulence, bed load sediment transport, and bed morphology, *J. Geophys. Res.*, *111*, F04007, doi:10.1029/2005JF000458.

Celik, A., P. Diplas, C. Dancey, and M. Valyrakis (2010), Impulse and particle dislodgement under turbulent flow conditions, *Phys. Fluids*, *22*(4), doi:10.1063/1.3385433.

Chen, Z., A. Ortiz, L. J. Zong, and H. Nepf (2012), The wake structure downstream of a porous obstruction with implications for deposition near a finite patch of emergent vegetation, *Water Resour. Res.*, *48*, W09517, doi:10.1029/2012WR012224.

Chen, Z., C. Jiang, and H. Nepf (2013), Flow adjustment at the leading edge of a submerged aquatic canopy, *Water Resour. Res.*, *49*, 5537–5551, doi:10.1002/wrcr.20403.

Christiansen, T., P. L. Wiberg, and T. G. Milligan (2000), Flow and sediment transport on a tidal salt marsh surface, *Estuar. Coast. Shelf Sci.*, *50*(3), 315–331, doi:10.1006/ecss.2000.0548.

Church, M. (2006), Bed material transport and the morphology of alluvial river channels, *Annu. Rev. Earth Planet. Sci.*, *34*, 325–354, doi:10.1146/annurev.earth.33.092203.122721.

Ciraolo, G., G. B. Ferreri, and G. La Loggia (2006), Flow resistance of Posidonia oceanica in shallow water, *J. Hydraul. Res.*, *44*(2), 189–202, doi:10.1080/00221686.2006.9521675.

Clarke, S. J., and G. Wharton (2001), Sediment nutrient characteristics and aquatic macrophytes in lowland English rivers, *Sci. Total Environ.*, *266*(1–3), 103–112, doi:10.1016/S0048-9697(00)00754-3.

Corenblit, D., E. Tabacchi, J. Steiger, and A. M. Gurnell (2007), Reciprocal interactions and adjustments between fluvial landforms and vegetation dynamics in river corridors: A review of complementary approaches, *Earth Sci. Rev.*, *84*, 56–86.

Droppo, I. G. (2004), Structural controls on floc strength and transport, *Can. J. Civ. Eng.*, *31*, 569–578, doi:10.1139/l04-015.

Droppo, I. G., G. G. Leppard, D. T. Flannigan, and S. N. Liss (1997), The freshwater floc: A functional relationship of water and organic and inorganic floc constituents affecting suspended sediment properties, *Water Air Soil Pollut.*, *99*(1-4), 43–54, doi:10.1023/A:1018359726978.

Edwards, P. J., J. Kolmann, A. Gurnell, G. E. Petts, K. Tockner, and J. V. Ward (1999), A conceptual model of vegetation dynamics on gravel bars of a large alpine river, *Wetlands Ecol. Manage.*, *7*(3), 141–153, doi:10.1023/A:1008411311774.

Folkard, A. M. (2005), Hydrodynamics of model Posidonia oceanica patches in shallow water, *Limnol. Oceanogr.*, *50*(5), 1592–1600, doi:10.4319/lo.2005.50.5.1592.

Folkard, A. M. (2011), Flow regimes in gaps within stands of flexible vegetation: Laboratory flume simulations, *Environ. Fluid Mech.*, *11*(3), 289–306, doi:10.1007/s10652-010-9197-5.

Follett, E. M., and H. M. Nepf (2012), Sediment patterns near a model patch of reedy emergent vegetation, *Geomorphology*, *179*, 141–151, doi:10.1016/j.geomorph.2012.08.006.

Fuller, R., S. Doyle, L. Levy, J. Owens, E. Shope, L. Vo, E. Wolyniak, M. Small, and M. Doyle (2011), Impact of regulated releases on periphyton and macroinvertebrate communities: The dynamic relationship between hydrology and geomorphology in frequently flooded rivers, *River Res. Appl.*, *27*(5), 630–645, doi:10.1002/rra.1385.

Furukawa, K., E. Wolanski, and H. Mueller (1997), Currents and sediment transport in mangrove forests, *Estuar. Coast. Shelf Sci.*, *44*(3), 301–310, doi:10.1006/ecss.1996.0120.

Ghisalberti, M., and H. Nepf (2002), Mixing layers and coherent structures in vegetated aquatic flows, *J. Geophys. Res.*, *107*(C2), 3011, doi:10.1029/2001JC000871.

Gurnell, A. M., G. E. Petts, D. M. Hannah, B. P. G. Smith, P. J. Edwards, J. Kollmann, J. V. Ward, and K. Tockner (2001), Riparian vegetation and island formation along the gravel-bed Fiume Tagliamento, Italy, *Earth Surf. Processes Landforms*, *26*(1), 31–62, doi:10.1002/1096-9837(200101)26:1 < 31::AID-ESP155 > 3.0.CO;2-Y.

Gurnell, A., K. Tockner, P. J. Edwards, and G. E. Petts (2005), Effects of deposited wood on the biocomplexity of river corridor, *Front. Ecol. Environ.*, *3*(7), 377–382, doi:10.1890/1540-9295(2005)003[0377:EODWOB]2.0.CO;2.

Gurnell, A., T. D. Blackall, and G. E. Petts (2008), Characteristics of freshly deposited sand and finer sediments along an island-braided, gravel-bed river: The roles of water, wind, and trees, *Geomorphology*, *99*(1-4), 254–269, doi:10.1016/j.geomorph.2007.11.009.

Gurnell, A. M., W. Bertoldi, and D. Corenblit (2012), Changing river channels: The roles of hydrological processes, plants and pioneer fluvial landforms in humid temperate, mixed load, gravel bed rivers, *Earth Sci. Rev.*, *111*(1-2), 129–141, doi:10.1016/j.earscirev.2011.11.005.

Hoover, T., L. Marczk, J. Richardson, and N. Yonemitsu (2010), Transport and settlement of organic matter in small streams, *Freshwater Biol.*, *55*(2), 436–449, doi:10.1111/j.1365-2427.2009.02292.x.

Jones, J., A. Collins, P. Naden, and D. Sear (2012), The relationship between fine sediment and macrophytes in rivers, *River Res. Appl.*, *28*(7), 1006–1018, doi:10.1002/rra.1486.

Larsen, L., J. Harvey, G. Noe, and J. Crimaldi (2009), Predicting organic floc transport dynamics in shallow aquatic ecosystems: Insights from the field, the laboratory, and numerical modeling, *Water Resour. Res.*, *45*, W01411, doi:10.1029/2008WR007221.

Leonard, L. A., and M. E. Luther (1995), Flow hydrodynamics in tidal marsh canopies, *Limnol. Oceanogr.*, *40*(8), 1474–1484, doi:10.4319/lo.1995.40.8.1474.

Lightbody, A. F., and H. Nepf (2006), Prediction of velocity profiles and longitudinal dispersion in emergent salt marsh vegetation, *Limnol. Oceanogr.*, *51*(1), 218–228, doi:10.4319/lo.2006.51.1.0218.

Luhar, M., J. Rominger, and H. Nepf (2008), Interaction between flow, transport and vegetation spatial structure, *Environ. Fluid Mech.*, *8*(5-6), 423–439, doi:10.1007/s10652-008-9080-9.

Luhar, M., and H. Nepf (2011), Flow induced reconfiguration of buoyant and flexible aquatic vegetation, *Limnol. Oceanogr.*, *56*(6), 2003–2017, doi:10.4319/lo.2011.56.6.2003.

Nelson, J. M., R. L. Shreve, S. R. McLean, and T. G. Drake (1995), Role of near-bed turbulence structure in bed load transport and bed form mechanics, *Water Resour. Res.*, *31*(8), 2071–2086, doi:10.1029/95WR00976.

Nepf, H. (2012), Flow and transport in regions with aquatic vegetation, *Annu. Rev. Fluid Mech.*, *44*, 123–142, doi:10.1146/annurev-fluid-120710-101048.

Nino, Y., and M. H. Garcia (1996), Experiments on particle-turbulence interactions in the near-wall region of an open channel flow: Implications for sediment transport, *J. Fluid Mech.*, *326*, 285–319, doi:10.1017/S0022112096008324.

Ortiz, A. C. (2012), *Investigating the Effect of a Circular Patch of Vegetation on Turbulence Generation and Sediment Deposition Using Four Case Studies*, pp. 116, MIT, Cambridge.

Papanicolaou, A., C. Kramer, A. Tsakiris, T. Stoesser, S. Bomminayuni, and Z. Chen (2012), Effects of a fully submerged boulder within a boulder array on the mean and turbulent flow fields: Implications to bedload transport, *Acta Geophys.*, *60*(6), 1502–1546, doi:10.2478/s11600-012-0044-6.

Pope, S. (2000), *Turbulent Flows*, Cambridge Univ. Press, New York.

Rodrigues, S., J. G. Breheret, J. J. Macaire, F. Moatar, D. Nistoran, and P. Juge (2006), Flow and sediment dynamics in the vegetated secondary channels of an anabranching river: The Loire River (France), *Sediment. Geol.*, *186*(1-2), 89–109, doi:10.1016/j.sedgeo.2005.11.011.

Rominger, J. T., A. F. Lightbody, and H. M. Nepf (2010), Effects of added vegetation on sand bar stability and stream hydrodynamics, *J. Hydraul. Eng.*, *136*(12), 994–1002, doi:10.1061/(asce)hy.1943-7900.0000215.

Sand-Jensen, K., and T. V. Madsen (1992), Patch dynamics of the stream macrophyte, Callitriche cophocarpa, *Freshwater Biol.*, *27*(2), 277–282, doi:10.1111/j.1365-2427.1992.tb00539.x.

Sand-Jensen, K., and M. L. Pedersen (2008), Streamlining of plant patches in streams, *Freshwater Biol.*, *53*(4), 714–726, doi:10.1111/j.1365-2427.2007.01928.x.

Schnauder, I., and H. L. Moggridge (2009), Vegetation and hydraulic-morphological interactions at the individual plant, patch and channel scale, *Aquat. Sci.*, *71*(3), 318–330, doi:10.1007/s00027-009-9202-6.

Scott, M., J. Friedman, and G. Auble (1996), Fluvial process and the establishment of bottomland trees, *Geomorphology*, *14*(327-339), doi:10.1016/0169-555X(95)00046-8.

Statzner, B., and R. Mueller (1989), Standard hemispheres as indicators of flow characteristics in lotic benthos research, *Freshwater Biol.*, *21*(3), 445–459, doi:10.1111/j.1365-2427.1989.tb01377.x.

Sukhodolova, T. A., and A. N. Sukhodolov (2012), Vegetated mixing layer around a finite-size patch of submerged plants: 1. Theory and field experiments, *Water Resour. Res.*, *48*, W10533, doi:10.1029/2011WR011804.

Tanaka, N., and J. Yagisawa (2010), Flow structures and sedimentation characteristics around clump-type vegetation, *J. Hydro-environ. Res.*, *4*(1), 15–25, doi:10.1016/j.jher.2009.11.002.

Tsujimoto, G. (1999), Fluvial processes in streams with vegetation, *J. Hydraul. Res.*, *37*(6), 789–803, doi:10.1080/00221689909498512.

Valiela, I., J. Teal, and W. Deuser (1978), The nature of growth forms in the salt marsh grass *Spartina alterniflora*, *Am. Nat.*, *112*(985), 467–470.

Vandenbruwaene, W., et al. (2011), Flow interaction with dynamic vegetation patches: Implications for biogeomorphic evolution of a tidal landscape, *J. Geophys. Res.*, *116*, F01008, doi:10.1029/2010JF001788.

van Katwijk, M., A. Bos, D. Hermus, and W. Suykerbuyk (2010), Sediment modification by seagrass beds: Muddification and sandification induced by plant cover and environmental conditions, *Estuar. Coast. Shelf Sci.*, *89*(2), 175–181, doi:10.1016/j.ecss.2010.06.008.

van Wesenbeeck, B. K., J. van de Koppel, P. M. J. Herman, and T. J. Bouma (2008), Does scale-dependent feedback explain spatial complexity in salt-marsh ecosystems?, *Oikos*, *117*(1), 152–159, doi:10.1111/j.2007.0030-1299.16245.x.

White, B., and H. Nepf (2007), Shear instability and coherent structures in shallow flow adjacent to a porous layer, *J. Fluid Mech.*, *593*, 1–32, doi:10.1017/S0022112007008415.

Williams, J. J., P. D. Thorne, and A. D. Heathershaw (1989), Measurements of turbulence in the benthic boundary layer over a gravel bed, *Sedimentology*, *36*(6), 959–971, doi:10.1111/j.1365-3091.1989.tb01533.x.

Zong, L. J., and H. Nepf (2010), Flow and deposition in and around a finite patch of vegetation, *Geomorphology*, *116*(3-4), 363–372, doi:10.1016/j.geomorph.2009.11.020.

Zong, L. J., and H. Nepf (2011), Vortex development downstream of a finite porous obstruction in a channel, *J. Fluid Mech.*, *691*, 24, doi:10.1017/jfm.2011.479.